Photoevaporative Winds in the IM Lup Protoplanetary Disk

Evidence from the Low-SNR Regime

Thomas James Maher

This thesis is submitted in partial completion of the requirements of the
BS Astronomy-Physics Major

Advisors: L. Ilsedore Cleeves, Charles J. Law
Department of Astronomy
University of Virginia
May 13, 2024

Photoevaporative Winds in the IM Lup Protoplanetary Disk: Evidence from the Low-SNR Regime

Thomas James Maher*

May 13, 2024

Abstract

The IM Lup protoplanetary disk is a promising candidate for the first unambiguous observational detection of a photoevaporative wind. I provide context for the search for disk dissipation mechanisms, motivate the search for a dispersive photoevaporative wind in IM Lup using CI emission as a tracer and outline its current status, and present evidence from a matched filter analysis that detects CI at large radii despite noisy data. This detection justifies further observations to confirm the extended CI, and search directly for velocity perturbations deviating from Keplerian orbits. I conclude by outlining an observational proposal that I led as Principal Investigator in the April 2024 ALMA Cycle 11 open call, along with a proposed analysis plan.

1 Introduction

Star formation begins with interstellar molecular clouds of gas and dust with mass, volume, and density on the order of $10^3\,\mathrm{M}_\odot$, $10\,\mathrm{pc}^3$, and $10^2\,\mathrm{cm}^{-3}$, respectively (Visser, 2014). These clouds have natural regions of higher density than the average, called clumps, filaments, and cores. Cores, which are typically on the order of $10^2\,\mathrm{M}_\odot$ and 1/10th of a parsec, are the most dense of these regions, with densities on the order $10^4 - 10^5\,\mathrm{cm}^{-3}$. Ordinarily, such cloud cores are in hydrostatic equilibrium, with pressure balancing gravity. However, at a certain critical scale, the equilibrium is broken and gravity dominates, causing collapse. The mass and radius at which collapse occurs are the so-called the Jeans mass and the Jeans length. The Jeans length can also be interpreted as the critical wavelength for oscillations caused by density perturbations (i.e., the shockwave from a nearby supernova), above which collapse is triggered (Krumholtz, 2016).

*Thanks to my advisors Charles J. Law and Ilse Cleeves for their time, instruction, guidance, advice, and patience, and to the rest of the Cleeves Group for their acceptance and support.

Collapsing cloud cores form pre-stellar cores. After 10^4—10^5 years, these pre-stellar cores become protostars. At 10^6 years, these protostars become T Tauri stars. The remaining material (gas, dust, and ice) not directly used in star formation forms a circumstellar disk. This flattening occurs because: (i) the cloud has some initial angular momentum in a 2D plane that is conserved, (ii) angular momentum conservation causes material to "spin out" in this plane as gravitational infall occurs and radial distance decreases, and (iii) motion along the free spatial axis averages out to zero due to energy loss from collisions (this process is common astrophysically, and can be observed in, for example, accretion disks and spiral galaxies).

With some exceptions – such as silhouette disks in the Orion Nebula Cluster (ONC) – disks are difficult to observe in the optical, but beginning in the early 2000s direct the advent of ground-based millimeter (mm) and sub-millimeter interferometers, in particular the Atacama Large Millimeter/submillimeter Array (ALMA) in Chile, enabled imaging of gas and dust contributions. It is clear through such observations that disk material is dispersed and cleared as the T Tauri star evolves into a pre-main sequence and then main sequence. For stars >5 Myr of age, are almost all gone (Pascucci and Tachibana, 2010).

Material can be removed from the disk through (i) planet formation, (ii) accretion onto the star, and (iii) dispersal out of the system. Here, I investigate option (iii). The timescale and physical mechanism of dispersal is an important open question in research into planet formation and evolution, since what types of planets can be formed is affected by the available mass reservoir and the nature of the available material, which will in turn determined by the precise nature of dispersal. Thus, this investigation has important consequences for characterizing not only disk evolution, but is also strongly linked to the creation and evolution of planetary systems.

Here, I investigate a type of possible disk wind known as a *photoevaporative* wind. External photoevaporation occurs when photons in the far ultraviolet (FUV) and extreme ultraviolent (EUV) portions of the electromagnetic spectrum raise the temperature of particles in the disk. It is a well-known result in statistical mechanics that the root-mean-square velocity of an ensemble of particles increases as $T^{1/2}$. Thus, the increase in temperature results in an increase in thermal motion, which, at large enough disk radii where the force of gravitational attraction is sufficiently small, results in particles reaching escape velocity and creating an outflow.

When the system is isothermal, setting the speed of sound in the material equal to the escape velocity yields the gravitational radius, R_g:

$$R_g = \frac{GM_*}{c_s^2} \tag{1}$$

Beyond R_g, material is gravitationally unbound. External irrational irradiation increases temperature

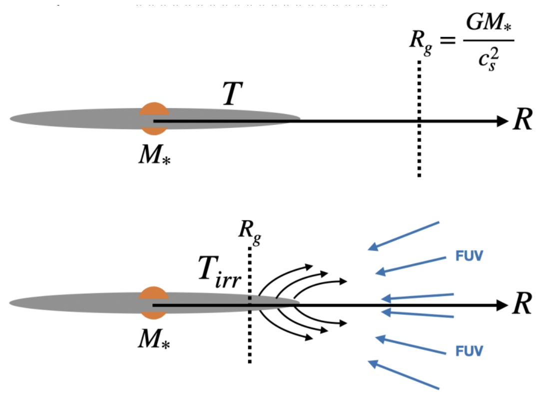

Figure 1: A schematic of external photoevaporation in terms of the gravitational radius (Winter and Haworth, 2022).

and thus increases c_s, resulting in a corresponding decrease in R_g. Should the gravitational radius decrease to sufficiently small values, it moves interior to the edge of the disc. This results in the gravitational unbinding of the outer material, which is then lost in an outward wind (Winter and Haworth, 2022); see Fig. 1.

Photoevaporation has already been observed for a special class of ionized protoplanetary disks in massive and densely clustered regions like the ONC, called proplyds. In fact, another open question is the so-called "proplyd lifetime problem," which refers to fact that photoeavaporation-driven mass-loss rates for proplyds in the ONC are so rapid that they imply that the disks were initially implausibly massive or that the source of the radiation, θ^1C Ori, is implausibly young (Winter et al., 2019). But while there are strong theoretical and observational hints to their existence, photoevaporative winds have yet to be detected in a "standard" protoplanetary disks in less intense UV environments. The first unambiguous observational detection of a photoevaporative wind would thus be a major step forward in our understanding of the evolution of stars and their associated disks and planetary systems. As I will outline later, this particular detection would prove this dispersal mechanism cannot be neglected even in low-mass star forming regions.

2 The State of the Search: CI Kinematic Tracers in IM Lup

IM Lupi (hereafter abbreviated IM Lup) is a young (≈ 1 Myr), approximately Solar-mass T Tauri star in the Lupus star-forming region, located in the constellation Lupus $(+15^h56^m09.23^s, -37°56', 05.9'')$ and at a distance of roughly d = 158 pc. It hosts a large protoplanetary disk radially extended for roughly 260 au in mm dust and for roughly 1000 au in ^{12}CO emission (Öberg et al., 2021). The disk is inclined at 48º and is vertically flared. (For clarity, "IM Lup" will be used to refer to the disk rather than the star for the rest of this paper.)

IM Lup is an ideal observational target for photoevaporative wind detection, due to its structure, favorable geometry, and the fact that it has been extensively modeled. Although located in a low mass cluster with a comparatively weak external UV radiation field – at least 10^4 times weaker than the field irradiating proplyds near O stars in the ONC – IM Lup's large size extent results in material at greater radii (> 400 AU) being weakly bound to the T Tauri star gravitationally, allowing significant mass loss to be induced (Haworth et al., 2017). Further, Law et al. (2021) find that the disk is vertically-flared, meaning the outer layers are directly exposed to stellar irradiation. The fact that IM Lup is large, close-by, vertically flared, and at a favorable inclination means it is straightforward to resolve the full 3D structure of bright elevated, such of that of CI emission (more on that shortly). Additionally, comprehensive physical and chemical models for the disk structure have already been developed for the disk structure by Cleeves et al. (2016) and Zhang et al. (2021). The physical structure is therefore well-constrained, which in turn means parameters for interpreting spectroscopic observations (e.g., gas and dust distributions, gas temperatures, gas abundances, gas optical depths, and the incident external radiation field) are likewise well-constrained. There is thus a clear framework for interpreting our results, and baseline to which they can be compared.

The aforementioned spectroscopic observations refer to the high-frequency forbidden lines of neutral atomic carbon (CI), which can be readily detected by ALMA. Since its initial discovery in the DM Tau disk by Tsukagoshi et al. (2015), the atomic-to-molecular [CI] $^3P_1 - ^3P_0$ or [CI] $1-0$ transition has been detected in several additional disks with ALMA: Pascucci et al. (2023) find it to be present in six of 10 large (r > 200 au) T Tauri disks in the Lupus region, while Urbina et al. (2024) go farther and spatially resolve the radial and vertical structure. An analysis of archival observations by Law et al. (2023) found CI in IM Lup specifically, using data from ALMA archival project 2015.1.01137.S (PI: T. Tsukagoshi). Based on these data, CI is expected to occupy a thin PDR-like vertical region between the CO photodissociation and carbon ionization fronts. Unlike other commonly-observed disk molecules, CI acts as a tracer of disk dynamical features, such as strong polar flows potentially associated with protoplanets (Alarcón et al., 2022), infalling streams associated with pebble drift (Sturm et al., 2022), and, most importantly, external photoevaporation (Haworth and Owen, 2020).

Haworth and Owen (2020) develop models of IM Lup using dynamical flow structure determined by the `torus-3dpdr` code (Bisbas et al., 2015) and thermal chemistry set by using a `healpix` scheme (Górski et al., 2005) to solve a PDR chemical network involving 3D line cooling (Bisbas et al., 2012). These models produce synthetic ALMA observations showing that, in the presence of a photoevaporative wind, CI will exhibit obvious deviations from would otherwise be expected given standard Keplerian rotation. In particular, CI position-velocity (PV) diagrams will show: (i) emission at greater than Keplerian speeds due to wind speeds, (ii) emission from upper-left and lower-right quadrants (not present in pure Keplerian diagrams) from the radial part of the wind on the disk's far and near sides. An illustrative PV diagram is showend in Fig. 2. These are distinguishable from

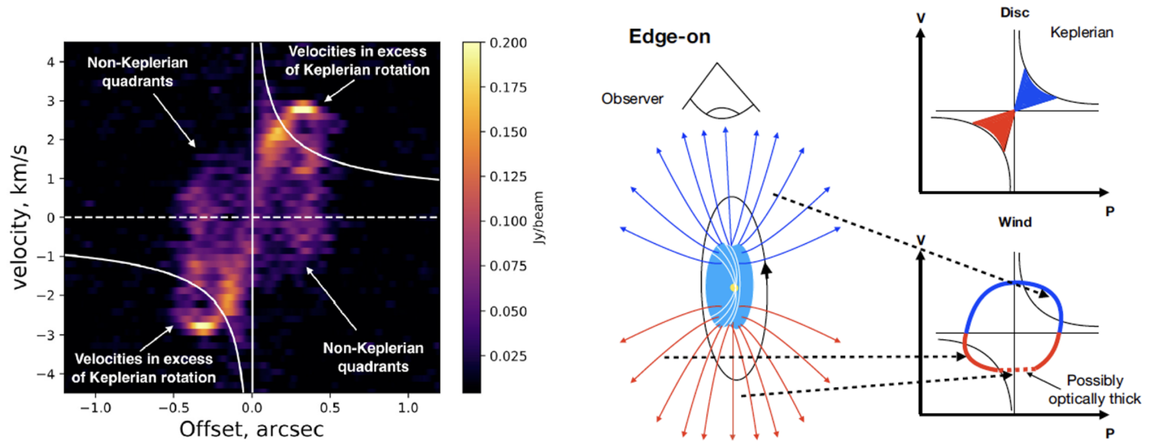

(a) A model PV diagram of CI emission in a protoplanetary disk at $i = 48°$, generated by Haworth and Owen (2020).

(b) A schematic from Haworth and Owen (2020) illustrating the relationship between CI emission morphology and disk geometry.

Figure 2: A synthetic CI PV diagram with an associated schematic to provide geometric intution.

inner photoevaporative winds driven by the star, since gas in the outer regions is significantly cooler. PV diagrams can be readily produced from ALMA data cubes using NRAO's Common Astronomy Software Applications (CASA) data processing software.

There is preliminary evidence for photoevaporation in IM Lup. Data from the ALMA Large Program Molecules with ALMA at Planet-forming Scales (MAPS) show that there is a large envelope-like ^{12}CO gas disk that extends to upwards of 1000 au (Zhang et al., 2021) as shown in Fig. 3a. Haworth et al. (2017) compare the radial extent of this ^{12}CO halo to the Cleeves et al. (2016) predictions and find that it does not match with hydrostatic chemical and radiative transfer models, as shown in Fig. 3b. The presence of a photoevaporative wind would explain the discrepancy, but unfortunately ^{12}CO is a poor kinematic tracer, since the deviation from Keplerian to the sub-Keplerian rotation associated with the ^{12}CO wind is subtle and difficult to detect at intermediate UV field strengths (Haworth and Clarke, 2019).

For the reasons mentioned above, the signatures of a photoevaporative wind would be clear and easier to detect in CI emission. Unfortunately, the Law et al. (2023) data is very noisy, with only moderate spatial resolution, low velocity resolution , and a low signal-to-noise ratio (SNR). The Band 8 IM Lup observations found in the archival data come from only nine minutes total integration time, centered in a spectral window with a frequency resolution of 244 kHz (≈ 0.15) km/s and a maximum recoverable scale (MRS) of $\approx 2''.8$. This limited MRS combined with low SNR results in the CI emission morphology's patchy appearance. Further, above $r \approx 600$ au, CI is not directly observed and

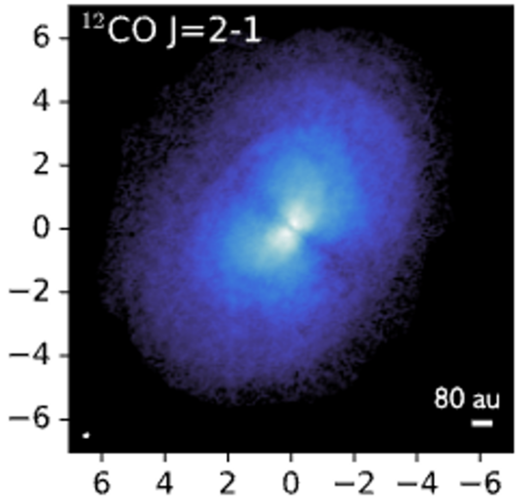

(a) Zeroth-moment map of ^{12}CO J=2–1 halo as observed by Zhang et al. (2021), extending out to ≈1000 au

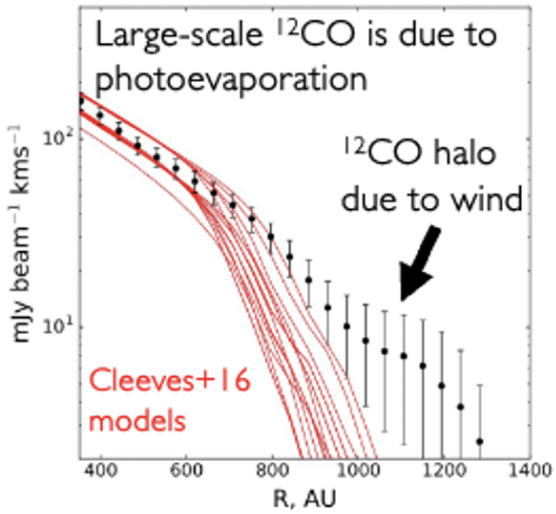

(b) Comparisons of ^{12}CO observations to existing models shows by Haworth and Owen (2020) show significant deviation.

Figure 3: An zeroth-moment map showing a ^{12}CO halo, compared against predicted radial extensions.

the SNR is very low, meaning the radial extent of CI emission appears significantly smaller than that of the ^{12}CO. This is illustrated in Fig. 4.

In summary, IM Lup is a prime candidate for observing photoevaporation. There is preliminary evidence from ^{12}CO emission, but ^{12}CO is a poor kinematic tracer of photoevaporative winds. CI is expected to be a much better tracer, but currently the data are not good enough to perform the analyses necessary for unambiguous detection. If there were some evidence that CI is present even in the more distant, low-SNR regime, this would justify a more intensive observational search, in order to obtain the better data required for mapping the kinematics, emission heights, and emission morphology out to large disk radii.

3 Overcoming Low SNR: Matched Filtering Analysis

Preliminary detection of CI emission in the noisy, large-radii regime is a first step that justifies investing telescope time in the further observations need to spatially and spectrally resolve the CI gas in the IM Lup disk in detail, which will enable us to detect and characterize the ongoing photoevaporation in this system, and unambiguously detect photoevaporative winds for the first time in general.

Matched filtering involves convolving a (conjugated, time-revereséd) known signal template, or filter, with a noisy signal, as shown in Fig. 5. In this case, the filter is the expected form of the CI data cube,

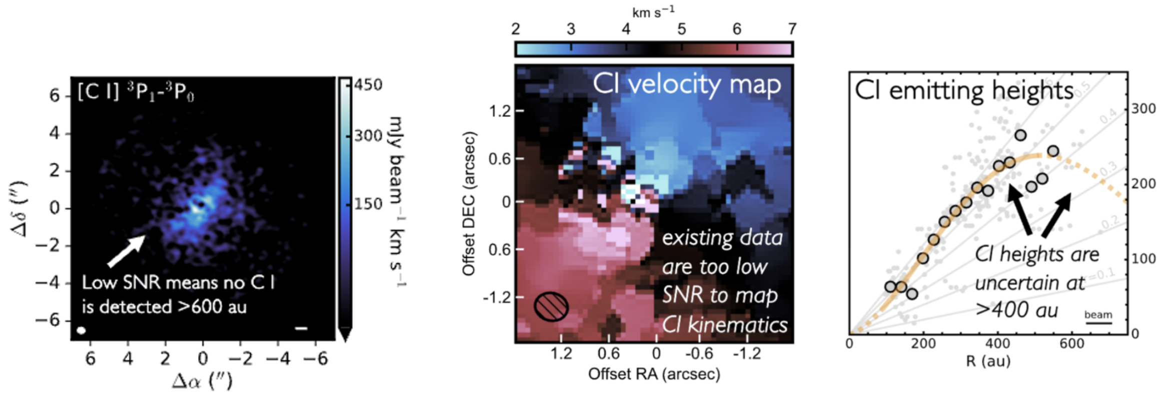

(a) The zeroth-moment map (in the same FOV as ^{12}CO) shows no CI detection for $r > 600$ au.

(b) The velocity map illustrates low SNR and difficult maping kinematic signatures.

(c) For $r > 400$ au, emitting heights for the CI are highly uncertain.

Figure 4: A zeroth-moment map, velocity map, and radius-dependent emitting height curve for CI emission in the IM Lup disk from Law et al. (2023).

and the signal is the 2015 ALMA archival data. The SNR is maximized when the form of the filter and the form of the signal are the closest match; the full derivation, which is omitted, leverages features of matrix algebra such as the definition of the inner product and the Cauchy-Schwartz inequality. I follow the techniques developed in Loomis et al. (2018) that leverage knowledge of the given source's structure and kinematics to increase sensitivity to weak spectral line observations. This method has shown to achieve an approximately 53% boost in SNR for CH_3OH detection in the TW Hya disk.

The matched filter analysis produces a one-dimensional impulse response spectrum T, of length $n_x - n_s + 1$. The elements of T at position i_0 are given by:

$$T_{i_0} = \sum_{i=i_o}^{i_0+N_S-1} x_i h_{i-i_0} \tag{2}$$

where $i_0 \in [0, n_x - n_s]$, $x = s + v$ is the sum of the signal s and some Gaussian noise v, and the filter kernel h is defined as:

$$h = \frac{1}{s^* R_v^{-1} s} R_v^{-1} s \tag{3}$$

The response T does not have physical significance but encodes the degree of similarity between the observations and the filter at any given point in the observed spectrum.

The matched filtering process used here proceeds in three steps, using three scripts. The first script, `keplerian_mask.py` builds the `make_mask` function. This function makes a Keplerian mask based on the imaging parameters, reading in image properties from an initial imaging run and then outputting a dirty image. The second script, `CLEAN_IMLup.py`, first runs the CASA `tclean` image reconstruction

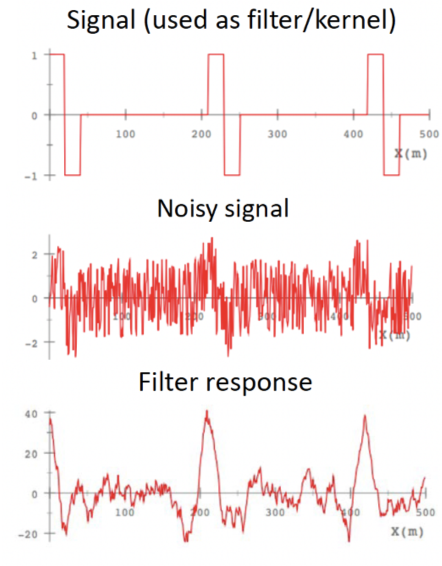

Figure 5: A visualization of matched filtering from Loomis (2018): the filter *(top)* is convolved against the noisy signal *(middle)*, producing the largest values for the filter response *(bottom)* when the form of the filter is closest to that of the signal.

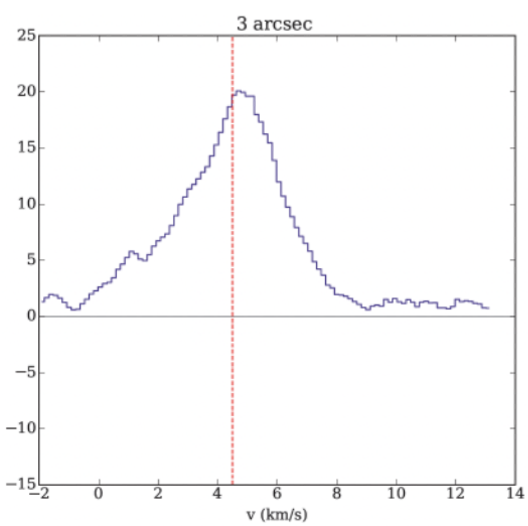

(a) Matched filter response for a circular mask with $r = 3''$

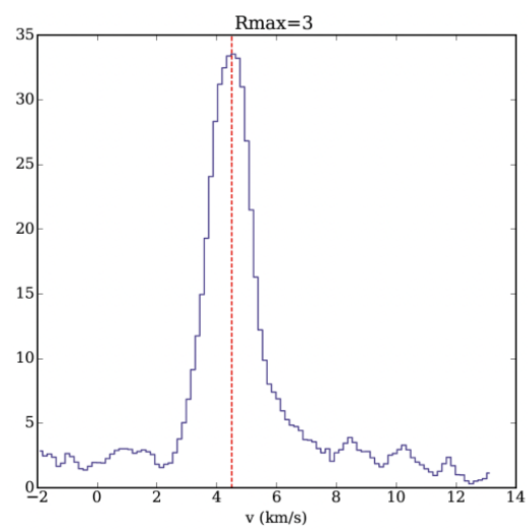

(b) Matched filter response for a non-annular Keplerian mask with $r = 3''$

Figure 6: The response is significantly greater for a Keplerian mask ($\approx 35\sigma$) vs. ($\approx 20\sigma$), indicating that Keplerian rotation is closer to the true morphology.

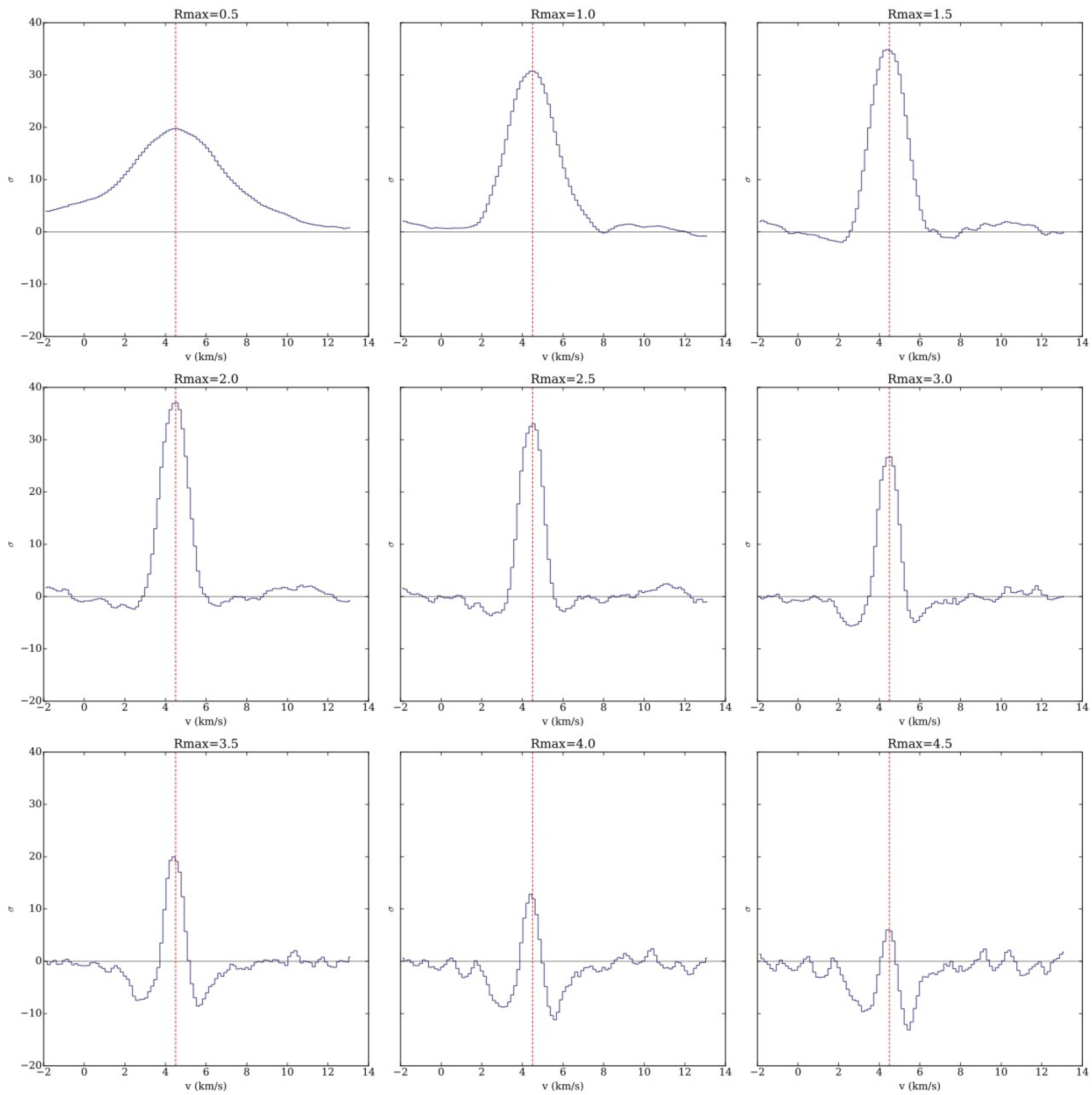

Figure 7: A 3×3 grid of matched filter response plots, using annular masks of $0.5''$ in width. The outer radius of the annuli begins at $0.5''$ and increases in $0.5''$ increments. Filter response σ is shown on the y-axis, velocity is shown on the x-axis. The systemic velocity $v_{\rm sys} = 4.5$ km/s is indicated with a red vertical line.

procedure on the dirty image, then calls the `make_mask` function to take the cleaned image, produce a Keplerian mask, and export the resultant mask as a .fits file. The script's disk parameters – distance, inclination, position angle, stellar mass, systemic velocity – are set to those of IM Lup. The (x_0, y_0) values are determined by `eddy` (Teague, 2019), and the position angle for the emission surface is extracted with `disksurf` (Teague et al., 2021). The mask is flat and has no spatial gradient.

The third script, `matched_filter.py`, executes the matched filter analysis and produces a graph of filter response as a function of velocity. This analysis applies the mask to directly to the measurement set of natively provided visibilities (i.e., the Fourier transform of the sky emission) from ALMA, since image reconstruction algorithms – the most common being `clean` (Briggs, 1995) – which are naturally imperfect reconstructions and can introduce artifacts.

The analysis relies on the open-source Python implementation of the `matched_filter()` method in `VISIBLE` package developed by Loomis et al. (2018), available under the MIT license at https://github.com/AstroChem/VISIBLE. Throughout this process, we have exploited the fact that the source inclination and position angle are often well-known and a spatiokinematic model of the gas can be approximated, meaning that an approximated matched filter that matches the parameters of CI can be generated to the be applied to the interferometric spectral line data to extract the signal.

If a mask with a particular morphology produces the (relative) best SNR in the matched filtering, it can be inferred that it is closer to the true morphology. Fig. 6 shows that the response is greater for Keplerian masks than circular masks, justifying the choice of Keplerian masks for the analysis. Fig. 7 shows the results of the completed matched filter analysis. The masks employed are annular "wedges" with Keplerian rotation, each with a width of $0.5''$, created by inputting the proper $r_{\max}$ and $r_{\min}$ parameters into the `CLEAN_IMLup` script. This is shown in Fig. 8a. The annular wedges begin at $r_{\max} = 0.5''$ in the upper left-hand corner. Going top to bottom, right to left, the maximum radius of the annulus increases radially outwards to $4.5''$. As expected, the filter response is largest within the observed 600 au radius. However, there is still significant matched filter response ($> 5\sigma$) up to $r = 4.5''$, (≈ 700 au), as shown in Fig. 8b over 100 au beyond where CI emission is seen in the initial image. there is therefore grounds for concluding that there is CI at large radii rotating at *at least* Keplerian speeds, with the possibility of greater than Keplerian speeds expected in the presence of photoevaporation.

4 Further Research

The matched filtering analysis reveals the presence of CI emission at greater radii than detected in the initial Law et al. (2023) image, there to be spatially and spectrally resolved with a more properly calibrated search. On this basis, I lead an ALMA Cycle 11 proposal submission requesting roughly five hours of observation time on IM Lup, in order to observe CI emission surface with better spatial

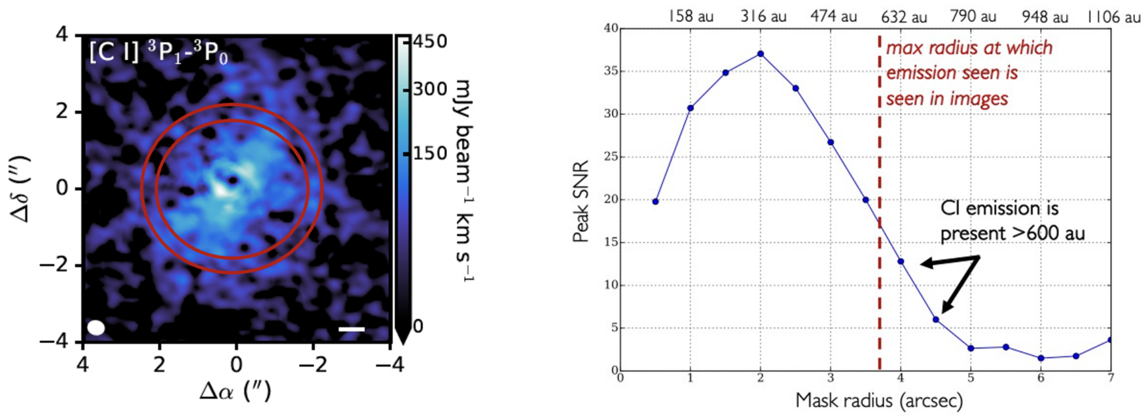

(a) An example of an annular mask applied to the CI data for matched filtering.

(b) A graph of peak matched filter response as a function of radius

Figure 8: An example of the annular Keplerian mask is shown on the right. On the left is a graph of peak SNR obtained as a function of mask radius; as indicated, there is significant $(5 - 10\sigma)$ filter response beyond > 600 au, beyond where CI is seen in images.

resolution, velocity resolution, depth, bandwidth, sensitivity, and SNR. The proposed observation targets [CI] 1-0 line in Band 8 (chosen over Band 10 for weather and scheduling reasons) for roughly one hour with the 43-antenna 12m array and 1.5 hours with the 7m Atacama Compact Array (ACA).

The requested correlator setup maximizes the velocity resolution at $74\,\mathrm{m/s}^{-1}$. This is an order of magnitude improvement over the Law et al. (2023) data, and well below the coarser maximum velocity resolution value required for the detection of wind signatures, suggested by the Haworth and Owen (2020) synthetic observations to be 150 m/s. Our proposal includes a total bandwidth of ≈ 140 km/s in order to capture potential fast CI wind components on the order of several 10s of km/s, as some models predict (Gressel et al., 2020). We request 20 mJy in 150 m/s channels, a depth of $5\times$ that of the existing data, which will correspondingly yield a much higher SNR of $> 25\sigma$.

The requested spatial resolution is $0.1''$ (≈ 15 au) will enable the resolution of localized kinematic deviations, which serve as tracers of both photoevaporation as well as other structures and mechanisms of potential scientific interest. Examples of the later include infalls of the kind found by Alarcón et al. (2022), as well as other small-scale substructures (e.g., rings, gaps, spiral arms, and non-axisymmetries). Due to the combination of one 7m and two 12m (C-6, C-3) set-ups, these observations will be additionally be sensitive to large spatial scales on the order of $\approx 10''$, a sensitivity necessitated by IM Lup's large angular extent.

Once these data have been obtained, the CI emitting surface can be determined using well-established methods such as `disksurf` and `alfahor` (Paneque-Carreño et al., 2023), which allow robust channel-by-channel visit of the vertical line emitting heights. These CI emitting heights will then be employed to deproject that CI velocity field using `eddy` to search for kinematic wind signatures. These signatures will be quantified and used to generate PV diagrams which can be compared against the deviations from Keplerian rotation expected when photoevaporation is occurring. Known velocity profiles, such as that of the high-resolution ^{12}CO data, can be subtracted to identify other deviations, an approach that has discovered local perturbations due to embedded planet candidates in the past.

5 Conclusion

Accurately characterizing disk dispersal mechanisms has key implications for our understanding of mass loss rates and the available mass reservoir in protoplanetary disks, a crucial piece of the full picture of planet formation. Outflowing photoevaporative winds are one such disperal mechanism, but they have yet to be detected outright. There are strong theoretical reason to believe neutral atomic carbon (CI) emission acts as unique kinematic tracer of external photoevaporation. There is strong preliminary evidence for the presence of CI at high radii in the IM Lup disk, bolstered by the matched filter analysis presented in this paper, giving us reason to be optimistic that future IM Lup observations will provide clearer evidence.

References

Alarcón, Felipe, et al. "A Localized Kinematic Structure Detected in Atomic Carbon Emission Spatially Coincident with a Proposed Protoplanet in the HD 163296 Disk." *The Astrophysical Journal Letters*, Vol. 941, No. 2 (2022)

Bisbas, T.G., et al. "3d-pdr: a new three-dimensional astrochemistry code for treating photodissociation regions." *Monthly Notices of the Royal Astronomical Society*, Volume 427, No. 3 (2012), pp. 2100–2118

Bisbas, T.G., et al. "torus-3dpdr: a self-consistent code treating three-dimensional photoionization and photodissociation regions." *Monthly Notices of the Royal Astronomical Society*, Vol. 454, No. 3 (2015), pp. 2828–2843

Briggs, Daniel Shannon. "High Fidelity Deconvolution of Moderately Resolved Sources." PhD Thesis, Department of Physics, New Mexico Institute of Mining and Technology

Cleeves, L. Ilsedore et al. "The Coupled Physical Structure of Gas and Dust in the IM Lup Protoplanetary Disk." *The Astrophysical Journal*, Vol. 832, No. 2 (2016)

Gressel, Oliver, et al. "Global Hydromagnetic Simulations of Protoplanetary Disks with Stellar Irradiation and Simplified Thermochemistry." *The Astrophysical Journal*, Vol. 896, No. 2 (2020)

GÓRSKI, K.M., et al. "HEALPix: A Framework for High-Resolution Discretization and Fast Analysis of Data Distributed on the Sphere." *The Astrophysical Journal*, Vol. 622, No. 2 (2005), pp. 759–771

HAWORTH, Thomas J., et al. "First evidence of external disc photoevaporation in a low mass star forming region: the case of IM Lup." *Monthly Notices of the Royal Astronomical Society: Letters*, Vol. 468, No. 1 (2017), pp. L108–L112

HAWORTH, Thomas J. & CLARKE, Cathie. "The first multidimensional view of mass loss from externally FUV irradiated protoplanetary discs." *Monthly Notices of the Royal Astronomical Society*, Vol. 485, No. 3 (2019), pp. 3895–3908

HAWORTH, Thomas J. & OWEN, James E. "The Observational Anatomy of Externally Photoevaporating Planet-Forming Discs I: Atomic Carbon." *Monthly Notices of the Royal Astronomical Society*, Vol. 492, No. 4 (2020), pp. 5030–5040

KRUMHOLTZ, Mark R. "Notes on Star Formation." Open Astrophysics Bookshelf, ArXiv:1511.03457v2 (2016)

LAW, Charles J., et al. "Molecules with ALMA at Planet-forming Scales (MAPS). IV. Emission Surfaces and Vertical Distribution of Molecules." *The Astrophysical Journal Supplement Series*, Vol. 257, No. 1 (2021)

LAW, Charles J., et al. "CI Traces the Disk Atmosphere in the IM Lup Protoplanetary Disk." *The Astrophysical Journal Letters*, Vol. 959, No. 2 (2023)

LOOMIS, Ryan. "Applications of Matched Filtering for Improved InterferometricImaging and Weak Line Detection." NRAO Presentation (2018)

LOOMIS, Ryan, et al. "Detecting Weak Spectral Lines in Interferometric Data through Matched Filtering." *The Astronomical Journal*, Vol. 155, No. 4 (2018)

ÖBERG, Karin I., et al. "Molecules with ALMA at Planet-forming Scales (MAPS). I. Program Overview and Highlights." *The Astrophysical Journal Supplement Series*, Vol. 257, No. 1 (2021)

PASCUCCI, Ilaria & TACHIBANA, Shogo. "The Clearing of Protoplanetary Disks and of the Protosolar Nebula." In Apai, D & Lauretta, D.S. (Eds.), *Protoplanetary Dust: Astrophysical and Cosmochemical Perspectives*" Cambridge University Press (2010), pp. 263–298

PASCUCCI, Ilaria, et al. "Large Myr-old Disks Are Not Severely Depleted of Gas-phase CO or Carbon." *The Astrophysical Journal*, Vol. 953, No. 2 (2023)

PANEQUE-CARREÑO, Teresa. "Directly tracing the vertical stratification of molecules in protoplanetary disks." *Astronomy & Astrophysics*, Vol. 669 (2023)

STURM, J.A. "Tracing pebble drift and trapping using radial carbon depletion profiles in protoplanetary disks." *Astronomy & Astrophysics*, Vol. 660 (2022)

TEAGUE, Richard. "EDDY: Extracting Protoplanetary Disk Dynamics with Python." *Journal of Open Source Software*, Vol. 4, No. 34 (2019)

TEAGUE, Richard, et al. "EDDY: Extracting Protoplanetary Disk Dynamics with Python." *Journal of Open Source Software*, Vol. 4, No. 34 (2021)

TSUKAGOSHI, Takashi, et al. "First Detection of [C I] ${}^3P_1 - {}^3P_0$ Emission from a Protoplanetary Disk." *The Astrophysical Journal Letters*, Vol. 802, No. 1 (2015)

URBINA, F., et al. "Vertical and radial distribution of atomic carbon in HD 163296." Forthcoming in *Astronomy & Astrophysics*, ArXiv:arXiv:2403.05042v (2024)

WINTER, Andrew J., et al. "A solution to the proplyd lifetime problem." *Monthly Notices of the Royal Astronomical Society*, Vol. 490, No. 4 (2019), pp. 5478–5493

VISSER, Ruud. "Star Formation: Chemistry as a Probe of Embedded Protostars." Frank N. Bash Symposium 2013: New Horizons in Astronomy, arXiv:1402.3229 (2014)

WINTER, Andrew J. & HAWORTH, Thomas J. "The external photoevaporation of planet-forming discs." *The European Physical Journal Plus*, Vol. 137 (2022)

ZHANG, Ke, et al. "Molecules with ALMA at Planet-forming Scales (MAPS). V. CO Gas Distributions." *The Astrophysical Journal Supplement Series*, Vol. 257, No. 1 (2021)